

CERN-EP-2024-071
06 March 2024

Search for prompt production of pentaquarks in charm hadron final states

LHCb collaboration[†]

Abstract

A search for hidden-charm pentaquark states decaying to a range of $\Sigma_c \bar{D}$ and $\Lambda_c^+ \bar{D}$ final states, as well as doubly-charmed pentaquark states to $\Sigma_c D$ and $\Lambda_c^+ D$, is made using samples of proton-proton collision data corresponding to an integrated luminosity of 5.7 fb^{-1} recorded by the LHCb detector at $\sqrt{s} = 13 \text{ TeV}$. Since no significant signals are found, upper limits are set on the pentaquark yields relative to that of the Λ_c^+ baryon in the $\Lambda_c^+ \rightarrow p K^- \pi^+$ decay mode. The known pentaquark states are also investigated, and their signal yields are found to be consistent with zero in all cases.

Submitted to Phys. Rev. D

© 2024 CERN for the benefit of the LHCb collaboration. CC BY 4.0 licence.

[†]Authors are listed at the end of this paper.

1 Introduction

Since the formulation of the quark model [1, 2], hadronic states beyond the conventional $q\bar{q}$ mesons and qqq baryons have been proposed. Hadrons with different combinations of quarks q and gluons g , such as pentaquarks ($q\bar{q}qqq$), tetraquarks ($q\bar{q}q\bar{q}$) [1, 2], six-quark H-dibaryons ($q\bar{q}q\bar{q}q\bar{q}$) [3], hybrids ($q\bar{q}g$) [4] and glueballs (ggg) [5] have been predicted by QCD-based models. The existence of such “exotic” hadrons had been debated for several years without a consensus being reached. In the early 2000s, new hadrons with unexpected features were observed, such as the $D_{s0}^*(2317)^+$ [6] and $\chi_{c1}(3872)$ [7] mesons, followed shortly after by the discovery of many other charmonium-like and bottomonium-like states. While it is still not possible to rule out firmly a conventional nature for the majority of such states, the observation of manifestly exotic hadrons such as the $Z_c(4430)^+$ meson [8], an electrically charged charmonium-like state, three P_c^+ baryons [9–11], with a minimal quark content $c\bar{c}uud$, and the T_{cc}^+ state [12, 13], a meson containing two charm quarks, established the existence of QCD exotics. Many models have been proposed to explain the exotic nature of such states: *hadronic molecules* [14, 15], whose constituents are color-singlet hadrons bound by residual nuclear forces; *tetraquarks and pentaquarks* [16, 17], bound states where diquarks and diantiquarks are building blocks; *hadro-quarkonium* [18], a cloud of light quarks and gluons bound to a heavy $Q\bar{Q}$ core state via van-der-Waals forces (Q represents a heavy quark, such as the b quark), and *threshold effects*, enhancements caused by threshold cusps or rescattering processes [19, 20]. An intriguing feature of many exotic hadrons is the proximity to hadron-hadron thresholds. For example, the three pentaquark states $P_c(4312)^+$, $P_c(4440)^+$ and $P_c(4457)^+$, observed in the $J/\psi p$ projection of $\Lambda_b^0 \rightarrow J/\psi p K^-$ decays [11], have masses that are just below the $\Sigma_c^+ \bar{D}^0$ and $\Sigma_c^+ \bar{D}^{*0}$ thresholds.¹ More experimental and theoretical scrutiny is required to understand if this is just coincidental or related to the internal structure of the states as bound systems of a baryon and a meson. As for the conventional hadrons, the observation of new decay modes can shed light on the binding mechanism of exotic hadrons. In addition, many models predict doubly-charmed pentaquark states, where doubly-charmed refers to a state with two units of charm quantum number, decaying to a range of $\Sigma_c D$ and $\Lambda_c^+ D$ combinations [21]. Excited Ξ_{cc} baryons could be observed in such final states as well [22].

This paper presents a search for the $P_c(4312)^+$, $P_c(4440)^+$ and $P_c(4457)^+$ baryons and other pentaquarks with hidden charm, meaning charm quantum number equal to zero, in the prompt $\Sigma_c \bar{D}^{(*)}$, $\Sigma_c^* \bar{D}^{(*)}$, $\Lambda_c^+ \bar{D}^{(*)}$, and $\Lambda_c^+ \pi \bar{D}^{(*)}$ mass spectra.² A search for pentaquarks containing two charm quarks has also been carried out in the $\Sigma_c D^{(*)}$, $\Sigma_c^* D^{(*)}$, $\Lambda_c^+ D^{(*)}$ and $\Lambda_c^+ \pi D^{(*)}$ mass spectra. Upper limits on the yields in these spectra relative to the $\Lambda_c^+ \rightarrow p K^- \pi^+$ normalisation channel are presented. The measurements are based on samples of proton-proton (pp) collision data corresponding to an integrated luminosity of 5.7 fb^{-1} at centre-of-mass energies of 13 TeV recorded by the LHCb experiment between 2016 and 2018.

¹The $\Sigma_c(2455)$ and $\Sigma_c(2520)$ baryons are referred to as Σ_c and Σ_c^* , respectively.

²The inclusion of charge-conjugate processes is implied throughout.

2 The LHCb detector

The LHCb detector [23, 24] is a single-arm forward spectrometer covering the pseudorapidity range $2 < \eta < 5$, designed for the study of particles containing b or c quarks. The detector includes a high-precision tracking system consisting of a silicon-strip vertex detector surrounding the pp interaction region, a large-area silicon-strip detector located upstream of a dipole magnet with a bending power of about 4 Tm and three stations of silicon-strip detectors and straw drift tubes placed downstream of the magnet. The tracking system provides a measurement of the momentum, p , of charged particles with a relative uncertainty that varies from 0.5% at low momentum to 1.0% at 200 GeV/ c . The minimum distance of a track to a primary pp collision vertex (PV), the impact parameter (IP), is measured with a resolution of $(15 + 29/p_T) \mu\text{m}$, where p_T is the component of the momentum transverse to the beam, in GeV/ c . Different types of charged hadrons are distinguished using information from two ring-imaging Cherenkov detectors. Photons, electrons and hadrons are identified by a calorimeter system consisting of scintillating-pad and preshower detectors, an electromagnetic and a hadronic calorimeter. Muons are identified by a system composed of alternating layers of iron and multiwire proportional chambers.

The online event selection is performed by a trigger, which consists of a hardware stage followed by a two-level software stage [25]. At the hardware trigger stage, events are required to have a muon with high p_T or hadron, photon or electron with high transverse energy in the calorimeters. In between the two software trigger stages, an alignment and calibration of the detector is performed in near real-time and their results are used in the trigger [26]. The same alignment and calibration information is propagated to the offline reconstruction, ensuring consistent and high-quality particle identification (PID) information between the trigger and offline software. The identical performance of the online and offline reconstruction offers the opportunity to perform physics analyses directly using candidates reconstructed in the trigger [27, 28]. This analysis exploits this by using D^0 , D^+ and Λ_c^+ candidates fully reconstructed in the trigger, as well as single pions for certain final states.

Simulated pp collisions are generated using PYTHIA [29] with a specific LHCb configuration [30]. Decays of hadronic particles are described by EVTGEN [31], in which final-state radiation is generated using PHOTOS [32]. The interaction of the generated particles with the detector, and its response, are implemented using the GEANT4 toolkit [33] as described in Ref. [34].

3 Selection

All signal mode combinations are listed in Table 1. It is interesting to note that the quark content of each of these states is comparable to the quark content of the $J/\psi p$ combination ($c\bar{c}uud$), since all combinations consist of only the up, down and charm quarks. In the selection process, open-charm hadrons are selected by the trigger. The Λ_c^+ baryon is reconstructed in the $\Lambda_c^+ \rightarrow pK^-\pi^+$ decay mode for both signal and normalisation channels, the D^0 meson in the decay $D^0 \rightarrow K^-\pi^+$ and the D^+ meson in the decay $D^+ \rightarrow K^-\pi^+\pi^+$. To improve the signal purity, stringent PID and vertex quality requirements are imposed. To further suppress the background in the Λ_c^+ decay mode, the gradient-boosted decision

Table 1: All possible combinations of Σ_c or Λ_c^+ baryons with $D^{(*)}$ mesons to produce the isospin multiplet. Combinations of Λ_c^+ baryons, pions and D mesons are also considered. From each $\Sigma_c D$ combination the corresponding $\Lambda_c^+ \pi D$ combination can be derived. The charge of the corresponding pentaquark state is given, along with the isospin, hypercharge and charm quantum numbers. The last column indicates whether a mode has an upper limit set in this paper. The combinations are split by the charm value.

Hadron 1	Hadron 2	Charge	I_3	Y	C	Limit Set
Λ_c^+	\bar{D}^0	+1	$1/2$	1	0	✓
Λ_c^+	D^-	0	$-1/2$	1	0	✓
Λ_c^+	D^{*-}	0	$-1/2$	1	0	✓
Σ_c^{++}	\bar{D}^0	+2	$3/2$	1	0	✓
Σ_c^{++}	D^-	+1	$1/2$	1	0	✓
Σ_c^{++}	D^{*-}	+1	$1/2$	1	0	×
Σ_c^0	\bar{D}^0	0	$-1/2$	1	0	✓
Σ_c^0	D^-	-1	$-3/2$	1	0	✓
Σ_c^0	D^{*-}	-1	$-3/2$	1	0	×
Σ_c^{*++}	\bar{D}^0	+2	$3/2$	1	0	✓
Σ_c^{*++}	D^-	+1	$1/2$	1	0	✓
Σ_c^{*++}	D^{*-}	+1	$1/2$	1	0	✓
Σ_c^{*0}	\bar{D}^0	0	$-1/2$	1	0	✓
Σ_c^{*0}	D^-	-1	$-3/2$	1	0	✓
Σ_c^{*0}	D^{*-}	-1	$-3/2$	1	0	✓
Λ_c^+	D^0	+1	$-1/2$	3	2	✓
Λ_c^+	D^+	+2	$1/2$	3	2	✓
Λ_c^+	D^{*+}	+2	$1/2$	3	2	✓
Σ_c^{++}	D^0	+2	$1/2$	3	2	×
Σ_c^{++}	D^+	+3	$3/2$	3	2	×
Σ_c^{++}	D^{*+}	+3	$3/2$	3	2	×
Σ_c^0	D^0	0	$-3/2$	3	2	×
Σ_c^0	D^+	+1	$-1/2$	3	2	×
Σ_c^0	D^{*+}	+1	$-1/2$	3	2	×
Σ_c^{*++}	D^0	+2	$1/2$	3	2	✓
Σ_c^{*++}	D^+	+3	$3/2$	3	2	✓
Σ_c^{*++}	D^{*+}	+3	$3/2$	3	2	×
Σ_c^{*0}	D^0	0	$-3/2$	3	2	✓
Σ_c^{*0}	D^+	+1	$-1/2$	3	2	✓
Σ_c^{*0}	D^{*+}	+1	$-1/2$	3	2	×

tree classifier trained on data for the analysis described in Ref. [35] is used. This identifies Λ_c^+ candidates with high efficiency by combining information on the vertex quality and the PID. The classifier is applied directly in the case of the modes involving a direct Λ_c^+ decay and is used as an input to the multivariate algorithm that is used to select Σ_c candidates in the $\Sigma_c \rightarrow \Lambda_c^+ \pi^\pm$ decay mode. In Fig. 1 the invariant mass distribution for each of these open-charm hadrons is shown. Candidate D^* (Σ_c) hadrons are built by combining the D^0 (Λ_c^+) candidates with a well-identified charged pion with p_T above 200 MeV/ c .

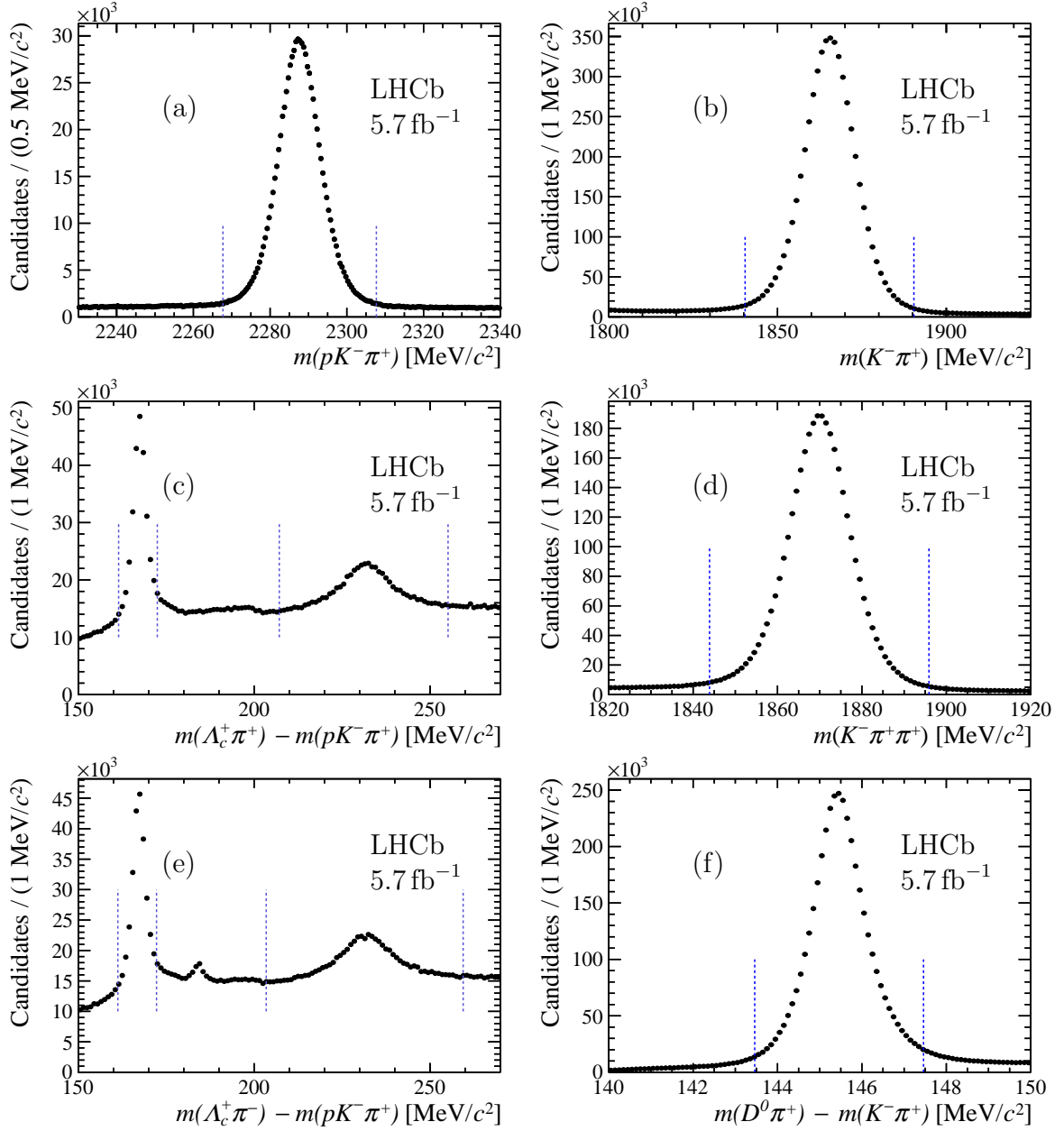


Figure 1: Invariant mass distributions of the (a) $\Lambda_c^+ \rightarrow pK^-\pi^+$, (b) $D^0 \rightarrow K^-\pi^+$, (c) $\Sigma_c^{(*)++} \rightarrow \Lambda_c^+\pi^+$, (d) $D^+ \rightarrow K^-\pi^+\pi^+$, (e) $\Sigma_c^{(*)0} \rightarrow \Lambda_c^+\pi^-$ and (f) $D^{*+} \rightarrow D^0\pi^+$ decays. Note that in (c), (e) and (f) the mass of the charm hadron is subtracted from the mass distribution to minimise detector resolution effects. In (e) a contribution can also be seen at around $185\text{ MeV}/c^2$ from the fully reconstructed $\Xi_c^0 \rightarrow \Lambda_c^+\pi^-$ decay. The blue dashed lines show the chosen signal windows around the peaks.

To improve the purity of the Σ_c selection, a multi-layer perceptron algorithm provided by the TMVA package [36] is trained using the $\Sigma_c^{++} \rightarrow \Lambda_c^+\pi^+$ simulated signal sample and a data sample at high mass, well above the expected signal, in order to describe the shape of the combinatoric background events. As input, the network uses the p_T and rapidity of the pion and of the Σ_c^{++} and Λ_c^+ baryons, together with information on the pion PID and the Λ_c^+ classifier response described above.

Once the corresponding baryon and meson combinations have been built, the signal regions are selected. These regions are based on fits to the baryon and meson spectra and require the mass is within a 3σ window around the mean mass value found from the fits, where σ is the resolution of the signal peak. These regions are dependent on the baryon and meson combination the signal mode consists of. The chosen windows are highlighted in Fig. 1. The background regions are selected as a wider window around the fitted mean value to accurately describe the background as close to the signal region as possible. This corresponds to a $3 - 4.5\sigma$ window around the fitted mean value of the mass. Selection criteria are applied on the opening angle between each pair of charged particles to ensure there are no candidates where the same track is used multiple times. If two or more candidates are selected, all but one candidate is discarded at random. Any signal combinations with fewer than 30 candidates within the mass range of interest are not analysed further. This corresponds to 10 modes in total, as summarised in Table 1. Note that all $\Lambda_c^+ D\pi$ combinations exceed this threshold.

4 Limit setting procedure

For each mode, a kinematic fit is done to constrain the mass of intermediate charm hadrons to their known values, and to constrain them to originate at the same PV. The Q -value spectrum, where the mass of each charmed hadron from the kinematic fit is subtracted from the decaying particle, is fitted using a simultaneous extended unbinned maximum-likelihood fit to the background and signal regions, where the background shape is shared between the two. The background normalisation region is a combination of the upper and lower sideband regions and for the $\Sigma_c D$ and $\Sigma_c^* D$ modes is selected from the Σ_c sideband region. For the $\Lambda_c^+ \pi D$ and $\Lambda_c^+ D$ modes the background region used is from the Λ_c^+ sideband region. For the $\Sigma_c D$, $\Sigma_c^* D$ and $\Lambda_c^+ \pi D$ modes, the background model used is a threshold function with all parameters shared between signal and sideband regions, while for the $\Lambda_c^+ D$ modes, the background model is the sum of a first-order Chebyshev polynomial and a log-normal distribution with all parameters shared between signal and sideband regions apart from the fraction between the two functions, which is independent. An example of the fit in the background-only hypothesis for each signal mode category ($\Sigma_c D$, $\Sigma_c^* D$, $\Lambda_c^+ D$ and $\Lambda_c^+ \pi D$) and the corresponding background is shown in Fig. 2. Four different signal models are investigated: one using a Gaussian function where the resolution is fixed to the detector resolution found using simulation, and three using Voigtian functions, built from the convolution of the same Gaussian function with a Breit–Wigner distribution, with fixed widths of 5, 10 and 15 MeV/c^2 , in order to provide greater sensitivity to pentaquark states with broader width. Larger widths are not considered, since the pentaquark states are predicted to be narrow [15].

The invariant mass distribution of $\Lambda_c^+ \rightarrow pK^- \pi^+$ candidates (the normalisation channel) is shown in Fig. 3. The distribution is fitted using the sum of a Gaussian function with a Crystal Ball function [37] for the signal model, and a first-order Chebyshev polynomial for the background. The obtained signal yield is $789\,200 \pm 1\,300$.

To search for possible pentaquark contributions, a scan of the Q -value distribution in each signal mode is made from the kinematic threshold up to $600 \text{ MeV}/c^2$ in steps of $4 \text{ MeV}/c^2$, which corresponds roughly to the signal resolution. At each point, an extended unbinned maximum-likelihood fit is performed. The local p -value is determined from the

difference between the negative log-likelihood of each fit and a fit with the background-only hypothesis and is assumed to be a one-tailed distribution. An example of the p -value distribution across the scan range is shown for each signal category for the $\Lambda_c^+ \pi^- \bar{D}^0$ mode in Fig. 4. The minimum local p -value in each channel varies from 0.041 in the $\Sigma_c^{*++} D^{*-}$ channel with the Voigtian signal model with a $15 \text{ MeV}/c^2$ width, to 3.36×10^{-6} in the $\Lambda_c^+ \pi^+ D^-$ channel with the Voigtian signal model with a $15 \text{ MeV}/c^2$ width. The latter corresponds to a local significance of 4.50σ .

The local p -value is corrected in order to account for the look-elsewhere effect [38] (LEE) using

$$p_{corr} = p_{loc} + \langle N(c_0) \rangle \exp\left(-\frac{c - c_0}{2}\right), \quad (1)$$

where p_{corr} and p_{loc} are the corrected and local p -value, respectively, c is the profile likelihood ratio $2\Delta \ln \mathcal{L}$, and c_0 is a reference level set to 0.5 where the average number of ‘upcrossings’ $\langle N(c_0) \rangle$ is found. An upcrossing is defined as when the profile likelihood ratio crosses the chosen threshold with a positive slope. The corrected p -value varies from 1 (corresponding to no observation of any significant signal) in many channels, to 1.45×10^{-4} in the $\Lambda_c^+ \pi^+ D^-$ channel with the Voigtian signal model where the width is set to $15 \text{ MeV}/c^2$. To evaluate the interpretation of these p -values the scanning procedure is repeated using 1000 background-only pseudo-experiments for each channel and the Voigtian signal model with a width of $15 \text{ MeV}/c^2$. The average number of fluctuations above 3σ significance across all channels is 7.0 with a standard deviation of 5.0. In the data, five channels, namely the $\Lambda_c^+ \pi^+ \bar{D}^0$, $\Lambda_c^+ \pi^+ D^-$, $\Lambda_c^+ \pi^- \bar{D}^0$, $\Lambda_c^+ \pi^- D^-$ and $\Lambda_c^+ \pi^- D^+$ channels, are observed with local significances greater than 3σ , obtained with the Voigtian signal model with a width of $15 \text{ MeV}/c^2$. Thus, we conclude that these significances are consistent with background fluctuations, as determined in the study with pseudo-experiments.

The previously observed pentaquark states are also investigated, namely the $P_c(4312)^+$, $P_c(4440)^+$ and $P_c(4457)^+$ states. This is only carried out for states with the same total charge and hidden charm quark content. By setting the mass and width in the Voigtian function to the known values of these states [11] and carrying out the same fitting procedure previously described, the significance of the states is found, and the limits are set using the procedure described below.

In this study, several sources of systematic uncertainties are considered. Since the number of tracks is different for signal and normalization, an important source of systematic uncertainty is due to the knowledge of the tracking efficiency, which is affected by hadronic interactions in the detector and overlaps between tracks or occupancy. Further uncertainties arise and are quantified from possible differences in the reconstruction between data and simulation, such as differences in selection and PID efficiencies. The performance of the classifier for the Σ_c baryon, and the behaviour of the trigger in data and simulation are also considered as sources of uncertainty. The knowledge of the branching fractions of the decay modes used leads to a further uncertainty [39]. The effect of varying the background model on the signal yield is also investigated, *e.g.* by using either a threshold function or Chebyshev polynomial summed with a log-normal distribution or by varying which background parameters are shared between the signal and background regions. This is done for the combination with the highest signal yield, and the uncertainty is applied for all signal combinations. The range of values found for each contribution is summarised in Table 2.

Table 2: Range of values of each systematic uncertainty contribution and the total combination for the different signal modes.

Source	Uncertainty (%)
Tracking	3.00 – 6.20
Reconstruction efficiency	0.70 – 3.70
Generation efficiency	0.10 – 0.20
Σ_c classifier performance	0.54
L0 trigger efficiency	1.40 – 7.90
Branching fraction	0.01 – 0.03
Background model	11.6
Total	12.10 – 15.79

An upper limit (UL) is set on $R(\Lambda_c^+)$, which is defined as

$$R(\Lambda_c^+) = \frac{N_P}{N_{\Lambda_c^+}} \times \frac{\epsilon_{\Lambda_c^+}}{\epsilon_P}, \quad (2)$$

where N represents the Λ_c^+ or pentaquark (P) yield and ϵ is the combined trigger and selection efficiency as found using simulated events. The limit is then determined at 90% and 95% confidence levels (CL). The likelihood profile is assumed to be parabolic, and is determined for five equal-sized steps in the signal yield around the value found from the fit. It is then convolved with a Gaussian function with a mean of zero and a width set to $\sigma = \sigma_{syst.} \cdot \mu$, where $\sigma_{syst.}$ is the systematic uncertainty on the signal yield and μ is the most probable signal yield. The convolved function takes the form

$$L(N') = \int_0^\infty L(N) \frac{1}{\sqrt{2\pi}\sigma} \exp\left(-\frac{(N - N')^2}{2\sigma^2}\right) dN, \quad (3)$$

where $L(N)$ is the normalised likelihood function. This likelihood profile is numerically integrated to find the value of the integral at 90% or 95% of the physical region, corresponding to the 90% and 95% CL upper limits on the signal yield and is then converted to an upper limit on $R(\Lambda_c^+)$ using Eq. 2. An example of the upper limit for each signal category is shown for the $\Lambda_c^+ \pi^- \bar{D}^0$ mode in Fig. 5.

The results for the scan across the Q -value spectrum in each signal combination are summarised in Appendix A. All channels show a signal yield consistent with the background-only hypothesis. The most significant deviation is seen in the $\Lambda_c^+ \pi^+ D^-$ channel. The fit result for this channel is shown in Fig. 6. When fitting with the mass and width of the known pentaquark states, the local significance in these spectra is found to be close to (or equal to) zero in all cases and is summarised in Table 3.

Table 3: Upper limits on $R(\Lambda_c^+)$ at 90% and 95% CL for the modes with the same total charge as the known pentaquark states, and with hidden-charm quark content. The local p -value and significance are listed as well as the signal yield, where the error on the signal yield is statistical only.

Decay Mode	Pentaquark Hypothesis	p -value	Significance (σ)	Signal Yield	Upper Limit ($\times 10^{-3}$)	
					(90% CL)	(95% CL)
$\Lambda_c^+ \bar{D}^0$	$P_c(4312)^+$	0.32	0.48	19.78 ± 22.27	1.17	1.29
	$P_c(4440)^+$	0.44	0.15	26.91 ± 28.17	1.41	1.53
	$P_c(4457)^+$	0.53	0.00	6.20 ± 13.60	1.27	1.43
$\Lambda_c^+ \pi^+ D^{*-}$	$P_c(4440)^+$	1.00	0.00	0.00 ± 0.96	0.72	0.91
	$P_c(4457)^+$	1.00	0.00	0.00 ± 1.73	0.77	0.97
$\Lambda_c^+ \pi^- D^{*-}$	$P_c(4440)^+$	1.00	0.00	0.00 ± 0.80	0.63	0.80
	$P_c(4457)^+$	1.00	0.00	0.00 ± 0.74	0.59	0.74
$\Lambda_c^+ \pi^+ D^-$	$P_c(4312)^+$	1.00	0.00	0.00 ± 1.56	0.69	0.88
	$P_c(4440)^+$	0.65	0.00	4.43 ± 11.67	3.71	4.24
	$P_c(4457)^+$	0.65	0.00	5.94 ± 12.68	3.13	3.61
$\Lambda_c^+ \pi^- D^-$	$P_c(4312)^+$	1.00	0.00	0.00 ± 1.42	0.67	0.86
	$P_c(4440)^+$	0.53	0.00	12.52 ± 15.89	3.91	4.37
	$P_c(4457)^+$	0.53	0.00	8.60 ± 12.22	3.10	3.51
$\Sigma_c^0 D^-$	$P_c(4440)^+$	1.00	0.00	0.00 ± 2.47	0.82	1.03
	$P_c(4457)^+$	1.00	0.00	0.00 ± 1.05	0.63	0.81
$\Sigma_c^{*0} D^-$	$P_c(4440)^+$	0.80	0.00	0.61 ± 4.52	1.13	1.37
	$P_c(4457)^+$	0.59	0.00	0.66 ± 1.79	0.80	0.99
$\Sigma_c^{*0} D^-$	$P_c(4440)^+$	0.31	0.49	3.23 ± 3.53	1.89	2.24
	$P_c(4457)^+$	1.00	0.00	0.00 ± 3.09	0.91	1.13
$\Sigma_c^{*++} D^-$	$P_c(4440)^+$	0.75	0.00	1.20 ± 3.81	1.38	1.67
	$P_c(4457)^+$	1.00	0.00	0.00 ± 5.74	0.87	1.08

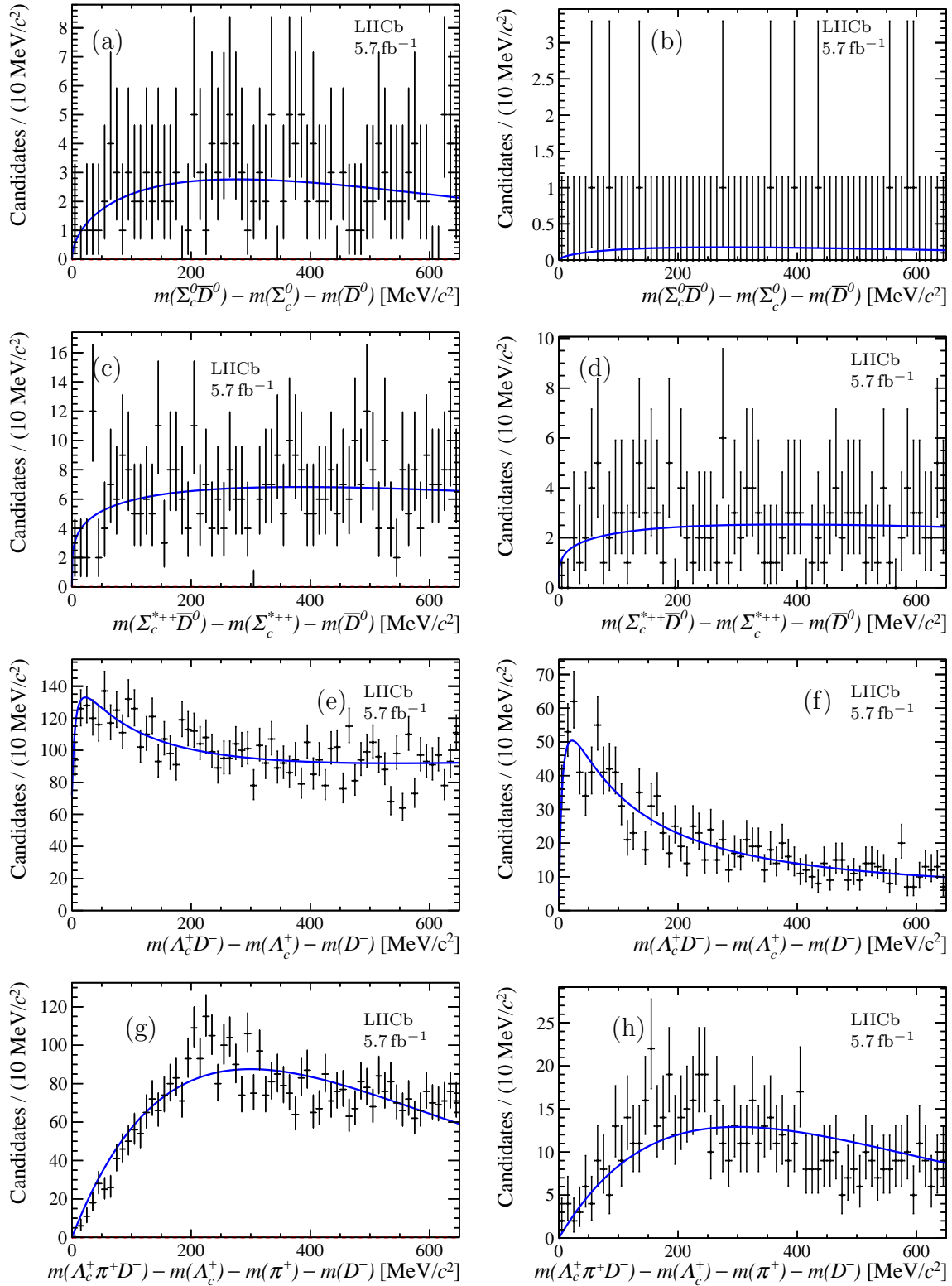


Figure 2: Distributions of the Q -value spectra for the $\Sigma_c^0 \bar{D}^0$ (a) signal and (b) background regions, for the $\Sigma_c^{*++} \bar{D}^0$ (c) signal and (d) background regions, the $\Lambda_c^+ D^-$ (e) signal and (f) background regions and the $\Lambda_c^+ \pi^+ D^-$ (g) signal and (h) background regions. The fits for the background-only hypotheses are overlaid.

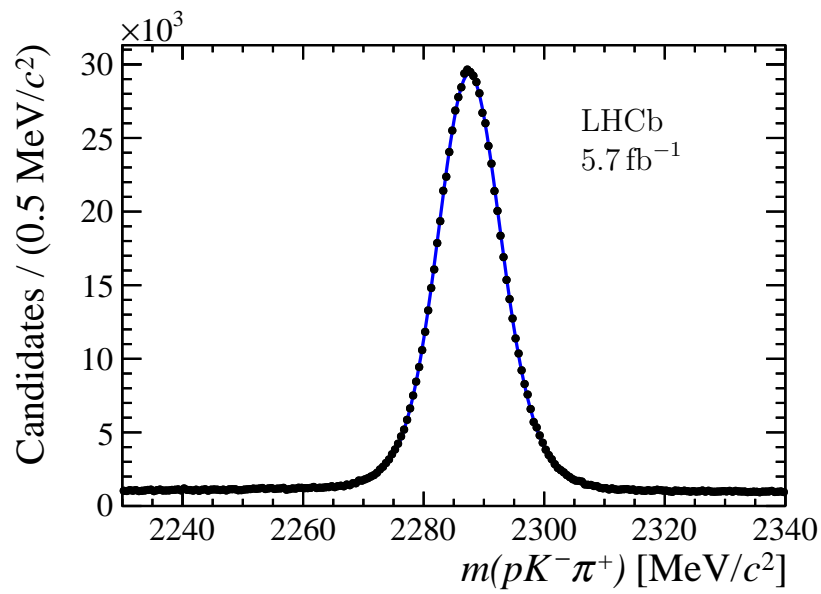


Figure 3: Invariant mass distribution of the $\Lambda_c^+ \rightarrow pK^-\pi^+$ decay. The fit results are overlaid.

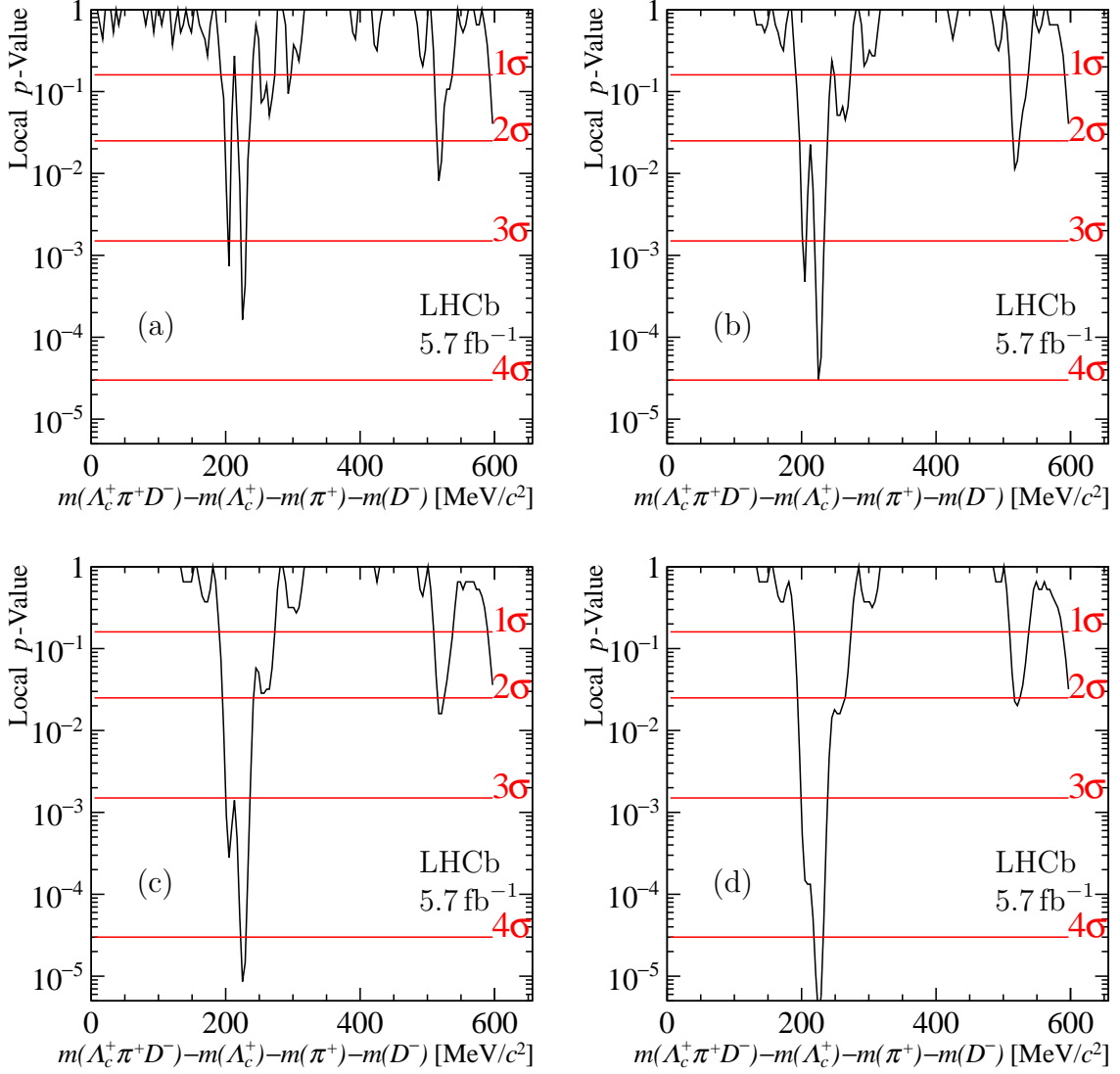


Figure 4: Local p -value distributions for the $\Lambda_c^+ \pi^+ D^-$ mode with different signal models: (a) Gaussian function, (b) Voigtian function with $5 \text{ MeV}/c^2$ width, (c) Voigtian function with $10 \text{ MeV}/c^2$ width, and (d) Voigtian function with $15 \text{ MeV}/c^2$ width. The red lines correspond to the levels of local significance.

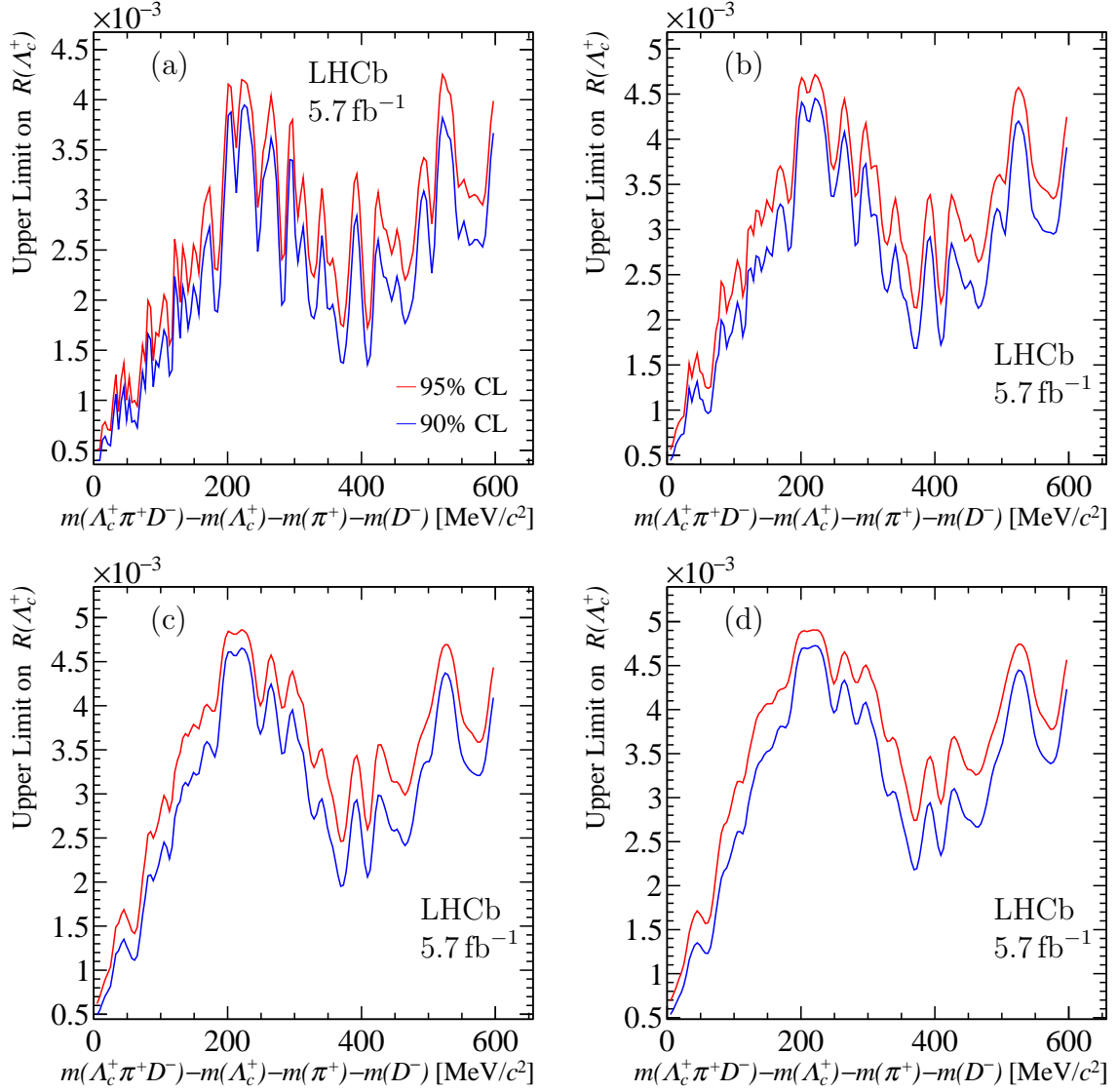


Figure 5: Upper limits on $R(\Lambda_c^+)$ distribution, at 90% and 95% CL, for the $\Lambda_c^+ \pi^+ D^-$ mode with different signal models: (a) Gaussian function, (b) Voigtian function with $5 \text{ MeV}/c^2$ width, (c) Voigtian function with $10 \text{ MeV}/c^2$ width, and (d) Voigtian function with $15 \text{ MeV}/c^2$ width.

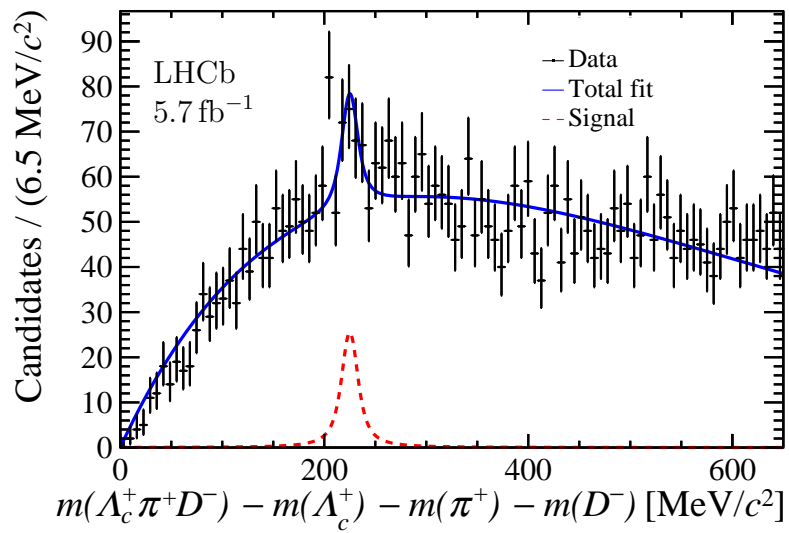


Figure 6: Distribution of the Q-value in the $\Lambda_c^+ \pi^+ D^-$ channel, where the most significant signal is seen. The fit result is overlaid.

5 Conclusion

Using an integrated luminosity of 5.7 fb^{-1} of pp collision data collected by the LHCb detector, a large range of combinations of open-charm and hidden-charm hadronic states are investigated for possible pentaquark decay channels. A signal model based on the known pentaquark states is also fitted, and the signal yield is found to be consistent with zero in all cases. When scanning the Q -value distribution from threshold to $600 \text{ MeV}/c^2$, the upper limit on the yield relative to the normalisation channel is set at 90% and 95% confidence levels. The highest significance is seen in the $\Lambda_c^+ \pi^+ D^-$ final state, however using studies of background-only pseudo-experiments this is found to be consistent with the background-only hypothesis.

Acknowledgements

We express our gratitude to our colleagues in the CERN accelerator departments for the excellent performance of the LHC. We thank the technical and administrative staff at the LHCb institutes. We acknowledge support from CERN and from the national agencies: CAPES, CNPq, FAPERJ and FINEP (Brazil); MOST and NSFC (China); CNRS/IN2P3 (France); BMBF, DFG and MPG (Germany); INFN (Italy); NWO (Netherlands); MNiSW and NCN (Poland); MCID/IFA (Romania); MICINN (Spain); SNSF and SER (Switzerland); NASU (Ukraine); STFC (United Kingdom); DOE NP and NSF (USA). We acknowledge the computing resources that are provided by CERN, IN2P3 (France), KIT and DESY (Germany), INFN (Italy), SURF (Netherlands), PIC (Spain), GridPP (United Kingdom), CSCS (Switzerland), IFIN-HH (Romania), CBPF (Brazil), and Polish WLCG (Poland). We are indebted to the communities behind the multiple open-source software packages on which we depend. Individual groups or members have received support from ARC and ARDC (Australia); Key Research Program of Frontier Sciences of CAS, CAS PIFI, CAS CCEPP, Fundamental Research Funds for the Central Universities, and Sci. & Tech. Program of Guangzhou (China); Minciencias (Colombia); EPLANET, Marie Skłodowska-Curie Actions, ERC and NextGenerationEU (European Union); A*MIDEX, ANR, IPhU and Labex P2IO, and Région Auvergne-Rhône-Alpes (France); AvH Foundation (Germany); ICSC (Italy); GVA, XuntaGal, GENCAT, Inditex, InTalent and Prog. Atracción Talento, CM (Spain); SRC (Sweden); the Leverhulme Trust, the Royal Society and UKRI (United Kingdom).

Appendices

A Summary tables

Tables 4, 5 and 6 summarise the upper limits set for each signal channel, along with the signal yields with corresponding significances, as well as the Q -value that these values occur at.

Table 4: Upper limits on $R(\Lambda_c^+)$ at 90% and 95% CL are shown for eleven of the hidden-charm modes, for their lowest p -value and highest significance (both local and corrected for LEE) found in the mass scan for all signal models. The Q -value and signal yield for these points are also summarised, where the error on the signal yield is statistical only.

Decay Mode	Width (MeV/ c^2)	Lowest p -value		Significance (σ)		Q -value (MeV/ c^2)	Signal Yield	UL ($\times 10^{-3}$)	
		Local	Corrected	Local	Corrected			90% CL	95% CL
$\Lambda_c^+ \bar{D}^0$	0	4.7×10^{-3}	0.36	2.60	0.36	353	22.7 ± 30.6	1.41	1.54
	5	3.4×10^{-3}	0.20	2.71	0.86	353	31.4 ± 12.8	1.53	1.64
	10	2.7×10^{-3}	0.13	2.78	1.15	349	39.4 ± 34.8	1.54	1.65
	15	2.2×10^{-3}	0.09	2.85	1.36	349	46.8 ± 91.0	1.57	1.67
$\Lambda_c^+ D^-$	0	4.7×10^{-3}	0.38	2.60	0.31	501	24.0 ± 12.9	2.05	2.25
	5	3.7×10^{-3}	0.22	2.67	0.77	497	26.7 ± 22.2	2.09	2.27
	10	2.7×10^{-3}	0.13	2.78	1.15	497	33.1 ± 23.0	2.17	2.35
	15	3×10^{-3}	0.11	2.75	1.21	497	38.0 ± 25.5	2.23	2.39
$\Lambda_c^+ D^{*-}$	0	1.4×10^{-3}	0.12	2.99	1.17	417	17.5 ± 6.9	2.48	2.72
	5	2.2×10^{-3}	0.13	2.85	1.13	417	20.8 ± 9.3	2.74	2.94
	10	3×10^{-3}	0.13	2.75	1.11	421	23.8 ± 9.6	2.80	2.96
	15	4.7×10^{-3}	0.16	2.60	0.99	421	26.3 ± 10.8	2.85	3.00
$\Sigma_c^{++} \bar{D}^0$	0	1.2×10^{-3}	0.10	3.04	1.27	301	7.0 ± 3.2	1.10	1.22
	5	4.3×10^{-3}	0.23	2.63	0.73	301	7.7 ± 3.6	1.23	1.37
	10	1.4×10^{-2}	0.48	2.21	0.04	301	7.9 ± 4.1	1.32	1.49
	15	3.2×10^{-2}	0.81	1.85	0.00	301	7.9 ± 4.5	1.40	1.59
$\Lambda_c^+ \pi^+ \bar{D}^0$	0	7.4×10^{-4}	0.06	3.18	1.58	245	41.9 ± 13.7	2.87	3.06
	5	9.69×10^{-5}	5.76×10^{-3}	3.73	2.53	245	67.6 ± 19.2	3.22	3.35
	10	2.46×10^{-5}	1.12×10^{-3}	4.06	3.06	245	91.6 ± 24.1	3.29	3.39
	15	8.61×10^{-6}	3.11×10^{-4}	4.30	3.42	245	115.0 ± 28.5	3.30	3.40
$\Sigma_c^{++} D^-$	0	5.2×10^{-3}	0.41	2.56	0.24	181	3.9 ± 2.3	1.07	1.21
	5	4.1×10^{-3}	0.22	2.65	0.76	177	6.8 ± 3.3	1.46	1.63
	10	3.7×10^{-3}	0.15	2.68	1.02	177	7.9 ± 3.7	1.64	1.84
	15	4.7×10^{-3}	0.15	2.60	1.03	177	8.4 ± 4.0	1.76	1.98
$\Lambda_c^+ \pi^+ D^-$	0	1.6×10^{-4}	0.01	3.59	2.21	225	41.6 ± 12.6	3.95	4.19
	5	3.03×10^{-5}	1.96×10^{-3}	4.01	2.89	225	64.7 ± 17.4	4.43	4.69
	10	8.61×10^{-6}	4.44×10^{-4}	4.30	3.32	225	87.1 ± 21.6	4.64	4.85
	15	3.36×10^{-6}	1.45×10^{-4}	4.50	3.62	225	108.2 ± 25.3	4.72	4.90
$\Lambda_c^+ \pi^+ D^{*-}$	0	2.7×10^{-3}	0.20	2.78	0.86	213	12.8 ± 5.3	3.42	3.75
	5	4.5×10^{-4}	0.02	3.32	1.96	213	22.3 ± 7.8	4.52	4.76
	10	1.45×10^{-4}	6.29×10^{-3}	3.62	2.50	213	30.4 ± 9.7	4.75	4.93
	15	7.42×10^{-5}	2.60×10^{-3}	3.79	2.79	209	37.7 ± 11.4	4.85	5.02
$\Sigma_c^0 \bar{D}^0$	0	1.3×10^{-2}	0.95	2.22	0.00	65	2.9 ± 2.0	0.68	0.78
	5	1.7×10^{-2}	0.79	2.13	0.00	65	3.7 ± 68.8	0.90	1.03
	10	2.2×10^{-2}	0.74	2.02	0.00	65	4.4 ± 4.3	1.02	1.18
	15	2.8×10^{-2}	0.74	1.90	0.00	65	4.8 ± 4.2	1.13	1.29
$\Lambda_c^+ \pi^- \bar{D}^0$	0	4.8×10^{-4}	0.04	3.30	1.72	597	54.0 ± 17.2	2.79	2.98
	5	9.65×10^{-5}	7.11×10^{-3}	3.73	2.45	597	78.8 ± 21.9	3.02	3.20
	10	2.71×10^{-5}	1.63×10^{-3}	4.04	2.94	597	104.0 ± 26.3	3.15	3.30
	15	9.50×10^{-6}	4.83×10^{-4}	4.28	3.30	597	128.5 ± 30.4	3.20	3.33
$\Sigma_c^0 D^-$	0	2.3×10^{-3}	0.19	2.84	0.88	261	4.4 ± 2.7	1.24	1.39
	5	3.4×10^{-3}	0.18	2.71	0.90	261	5.7 ± 3.0	1.50	1.69
	10	6×10^{-3}	0.23	2.51	0.74	261	6.4 ± 3.4	1.66	1.87
	15	1×10^{-2}	0.30	2.32	0.53	261	7.0 ± 3.8	1.78	2.03

Table 5: Upper limits on $R(A_c^+)$ at 90% and 95% CL are shown for eight of the hidden-charm modes, for their lowest p -value and highest significance (both local and corrected for LEE) found in the mass scan for all signal models. The Q -value and signal yield for these points are also summarised, where the error on the signal yield is statistical only.

Decay Mode	Width (MeV)	Lowest p -value		Significance (σ)		Q -value (MeV/ c^2)	Signal Yield	UL ($\times 10^{-3}$)	
		Local	Corrected	Local	Corrected			90% CL	95% CL
$A_c^+ \pi^- D^-$	0	3.9×10^{-4}	0.03	3.36	1.90	257	38.1 ± 12.4	4.28	4.56
	5	5.71×10^{-5}	3.33×10^{-3}	3.86	2.71	253	62.1 ± 17.1	4.62	4.83
	10	1.45×10^{-5}	6.92×10^{-4}	4.18	3.20	249	83.7 ± 21.2	4.72	4.88
	15	4.59×10^{-6}	1.83×10^{-4}	4.44	3.56	249	103.5 ± 24.6	4.77	4.92
$A_c^+ \pi^- D^{*-}$	0	4.4×10^{-3}	0.31	2.62	0.48	197	12.0 ± 5.3	3.11	3.45
	5	7.1×10^{-3}	0.31	2.45	0.51	197	16.8 ± 7.3	4.08	4.53
	10	8.6×10^{-3}	0.27	2.38	0.61	197	21.2 ± 9.1	4.69	5.15
	15	8.9×10^{-3}	0.22	2.37	0.78	197	25.5 ± 10.8	5.11	5.56
$\Sigma_c^{*++} \bar{D}^0$	0	1×10^{-2}	0.75	2.32	0.00	37	5.0 ± 2.8	0.96	1.09
	5	1.2×10^{-2}	0.62	2.24	0.00	37	7.8 ± 4.0	1.32	1.49
	10	2.7×10^{-2}	0.92	1.92	0.00	205	7.0 ± 20.6	1.57	1.78
	15	2.7×10^{-2}	0.73	1.92	0.00	485	12.5 ± 6.7	2.23	2.49
$\Sigma_c^{*++} D^-$	0	1.2×10^{-3}	0.11	3.03	1.21	537	6.5 ± 3.3	1.63	1.82
	5	1.6×10^{-3}	0.10	2.95	1.30	497	11.8 ± 5.0	2.52	2.79
	10	2.5×10^{-3}	0.11	2.81	1.24	497	13.0 ± 5.7	2.82	3.12
	15	4.3×10^{-3}	0.14	2.63	1.07	497	13.9 ± 6.3	3.02	3.37
$\Sigma_c^{*++} D^{*-}$	0	2.3×10^{-2}	1.40	2.00	0.00	193	2.5 ± 1.8	1.08	1.23
	5	3.5×10^{-2}	1.44	1.81	0.00	449	2.9 ± 2.1	1.26	1.45
	10	3.5×10^{-2}	1.08	1.81	0.00	453	3.2 ± 2.3	1.36	1.57
	15	4.1×10^{-2}	0.99	1.74	0.00	453	3.3 ± 2.4	1.45	1.66
$\Sigma_c^{*0} \bar{D}^0$	0	3.4×10^{-3}	0.27	2.71	0.63	341	11.4 ± 5.0	1.64	1.83
	5	2.6×10^{-3}	0.14	2.80	1.07	341	16.8 ± 6.8	2.29	2.56
	10	2.2×10^{-3}	0.09	2.84	1.31	341	21.3 ± 8.3	2.73	3.00
	15	1.8×10^{-3}	0.06	2.90	1.52	337	26.0 ± 9.6	3.02	3.27
$\Sigma_c^{*0} D^-$	0	7.2×10^{-3}	0.53	2.45	0.00	113	6.2 ± 3.2	1.44	1.62
	5	1.4×10^{-3}	0.08	2.99	1.40	537	11.5 ± 4.8	2.60	2.85
	10	1.1×10^{-3}	0.05	3.06	1.66	537	13.6 ± 5.4	2.99	3.27
	15	1.2×10^{-3}	0.04	3.02	1.70	537	15.1 ± 6.0	3.23	3.54
$\Sigma_c^{*0} D^{*-}$	0	9.9×10^{-3}	0.51	2.33	0.00	109	2.6 ± 1.7	0.96	1.11
	5	3.2×10^{-3}	0.16	2.73	0.99	17	2.8 ± 1.9	1.07	1.22
	10	4.1×10^{-3}	0.16	2.64	1.01	17	2.9 ± 2.1	1.13	1.30
	15	6.1×10^{-3}	0.17	2.51	0.94	17	3.0 ± 2.4	1.18	1.34

Table 6: Upper limits on $R(\Lambda_c^+)$ at 90% and 95% CL are shown for each doubly-charmed mode, for their lowest p -value and highest significance (both local and corrected for LEE) found in the mass scan for all signal models. The Q -value and signal yield for these points are also summarised, where the error on the signal yield is statistical only.

Decay Mode	Width (MeV)	Lowest p -value		Significance (σ)		Q -value (MeV/ c^2)	Signal Yield	UL ($\times 10^{-3}$)	
		Local	Corrected	Local	Corrected			90% CL	95% CL
$\Lambda_c^+ D^0$	0	8.2×10^{-3}	0.59	2.40	0.00	37	15.0 ± 7.3	0.97	1.06
	5	4.7×10^{-3}	0.26	2.60	0.64	153	26.8 ± 11.0	1.19	1.26
	10	2.7×10^{-3}	0.12	2.78	1.17	153	36.5 ± 14.0	1.27	1.35
	15	2.4×10^{-3}	0.09	2.82	1.34	153	45.0 ± 16.5	1.33	1.43
$\Lambda_c^+ D^+$	0	2×10^{-2}	1.43	2.05	0.00	133	9.4 ± 5.0	1.01	1.13
	5	4.7×10^{-3}	0.27	2.60	0.61	169	11.0 ± 9.9	1.25	1.41
	10	4.2×10^{-3}	0.18	2.64	0.90	169	13.5 ± 24.5	1.52	1.72
	15	5.8×10^{-3}	0.20	2.52	0.85	169	14.9 ± 7.6	1.71	1.92
$\Lambda_c^+ D^{*+}$	0	2.1×10^{-2}	1.25	2.04	0.00	29	3.5 ± 2.3	0.69	0.80
	5	1×10^{-2}	0.49	2.31	0.02	33	6.2 ± 4.2	1.15	1.32
	10	8.1×10^{-3}	0.31	2.41	0.51	33	8.8 ± 5.3	1.45	1.64
	15	7.1×10^{-3}	0.22	2.45	0.76	33	10.5 ± 6.2	1.66	1.88
$\Lambda_c^+ \pi^+ D^0$	0	2.7×10^{-3}	0.22	2.78	0.77	193	18.0 ± 7.2	2.02	2.19
	5	1.6×10^{-3}	0.09	2.95	1.32	193	28.0 ± 10.4	2.32	2.46
	10	1.4×10^{-3}	0.07	2.99	1.51	193	36.7 ± 12.9	2.46	2.62
	15	1.4×10^{-3}	0.05	2.99	1.61	197	44.8 ± 15.3	2.70	2.87
$\Lambda_c^+ \pi^+ D^+$	0	8.7×10^{-3}	0.49	2.38	0.03	225	12.2 ± 5.9	2.04	2.29
	5	2.5×10^{-3}	0.11	2.81	1.23	229	21.8 ± 8.5	3.05	3.32
	10	9.9×10^{-4}	0.03	3.09	1.81	229	29.1 ± 10.3	3.44	3.70
	15	5.9×10^{-4}	0.02	3.25	2.12	229	35.3 ± 11.9	3.70	3.96
$\Lambda_c^+ \pi^+ D^{*+}$	0	5.9×10^{-3}	0.39	2.52	0.28	77	1.9 ± 1.5	0.84	0.95
	5	4.5×10^{-3}	0.22	2.61	0.77	161	6.5 ± 3.6	1.81	2.04
	10	2.9×10^{-3}	0.11	2.76	1.23	161	9.2 ± 4.4	2.31	2.58
	15	1.5×10^{-3}	0.05	2.96	1.64	165	12.2 ± 5.1	2.80	3.10
$\Lambda_c^+ \pi^- D^0$	0	7.3×10^{-4}	0.06	3.18	1.53	593	20.3 ± 7.4	2.11	2.25
	5	6.6×10^{-4}	0.04	3.21	1.78	593	26.3 ± 9.3	2.26	2.38
	10	5.9×10^{-4}	0.03	3.24	1.95	593	32.3 ± 11.0	2.35	2.47
	15	4.8×10^{-4}	0.02	3.30	2.13	593	38.3 ± 12.5	2.42	2.54
$\Lambda_c^+ \pi^- D^+$	0	1.2×10^{-4}	0.01	3.67	2.32	153	21.4 ± 6.9	2.99	3.24
	5	2.07×10^{-5}	1.36×10^{-3}	4.10	3.00	153	33.3 ± 9.5	3.65	3.88
	10	9.44×10^{-6}	4.93×10^{-4}	4.28	3.29	153	43.1 ± 11.6	4.06	4.28
	15	5.96×10^{-6}	2.54×10^{-4}	4.38	3.48	153	51.7 ± 13.4	4.29	4.48
$\Lambda_c^+ \pi^- D^{*+}$	0	2.3×10^{-3}	0.17	2.84	0.97	73	3.2 ± 3.0	1.19	1.35
	5	6.8×10^{-4}	0.04	3.20	1.76	73	5.7 ± 3.3	1.71	1.92
	10	8.5×10^{-4}	0.04	3.14	1.79	73	7.0 ± 3.8	1.94	2.19
	15	1.3×10^{-3}	0.04	3.01	1.70	73	7.6 ± 4.2	2.10	2.36
$\Sigma_c^{*++} D^0$	0	1.2×10^{-2}	0.88	2.27	0.00	113	2.5 ± 1.8	0.63	0.72
	5	9.4×10^{-3}	0.50	2.35	0.00	113	3.2 ± 2.2	0.76	0.87
	10	1.3×10^{-2}	0.48	2.23	0.04	113	3.6 ± 2.4	0.87	1.00
	15	1.8×10^{-2}	0.52	2.11	0.00	113	3.9 ± 2.7	0.95	1.11
$\Sigma_c^{*++} D^+$	0	6×10^{-3}	0.48	2.51	0.05	133	1.9 ± 1.5	0.70	0.81
	5	6.8×10^{-3}	0.37	2.47	0.34	133	2.7 ± 1.9	0.89	1.02
	10	8.8×10^{-3}	0.34	2.37	0.41	133	3.0 ± 2.1	0.97	1.11
	15	1.2×10^{-2}	0.35	2.27	0.38	133	3.2 ± 2.2	1.03	1.18
$\Sigma_c^{*0} D^0$	0	1.52×10^{-5}	1.67×10^{-3}	4.17	2.93	89	3.9 ± 2.0	0.68	0.76
	5	5.13×10^{-5}	3.70×10^{-3}	3.88	2.68	89	5.3 ± 2.6	0.90	0.99
	10	1.06×10^{-4}	5.47×10^{-3}	3.70	2.54	89	6.2 ± 3.0	1.03	1.14
	15	1.66×10^{-4}	6.69×10^{-3}	3.59	2.47	89	6.8 ± 3.2	1.13	1.25
$\Sigma_c^{*0} D^+$	0	1.8×10^{-2}	1.20	2.10	0.00	325	2.6 ± 1.8	0.88	1.01
	5	1.3×10^{-2}	0.61	2.23	0.00	73	3.5 ± 2.4	1.12	1.29
	10	1.3×10^{-2}	0.48	2.21	0.06	73	3.8 ± 3.2	1.29	1.50
	15	1.5×10^{-2}	0.41	2.18	0.22	69	4.7 ± 3.7	1.51	1.75

References



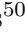




























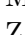



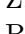
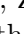


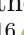

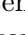
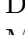
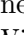


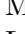

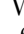

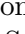
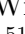
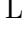


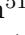
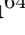


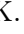


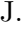
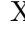

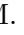


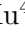





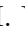


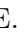









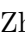
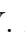

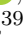
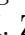


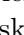

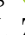
- [1] M. Gell-Mann, *A schematic model of baryons and mesons*, Phys. Lett. **8** (1964) 214.
- [2] G. Zweig, in *An $SU(3)$ model for strong interaction symmetry and its breaking. Version 2*, D. B. Lichtenberg and S. P. Rosen, eds., pp. 22–101, 1964.
- [3] R. L. Jaffe, *Perhaps a stable dihyperon*, Phys. Rev. Lett. **38** (1977) 195, Erratum *ibid.* **38** (1977) 617.
- [4] D. Horn and J. Mandula, *A model of mesons with constituent gluons*, Phys. Rev. **D17** (1978) 898.
- [5] H. Fritzsch, M. Gell-Mann, and H. Leutwyler, *Advantages of the color octet gluon picture*, Phys. Lett. **B47** (1973) 365.
- [6] BaBar collaboration, B. Aubert *et al.*, *Observation of a narrow meson decaying to $D_s^+\pi^0$ at a mass of $2.32\text{ GeV}/c^2$* , Phys. Rev. Lett. **90** (2003) 242001, [arXiv:hep-ex/0304021](#).
- [7] Belle collaboration, S. K. Choi *et al.*, *Observation of a narrow charmonium-like state in exclusive $B^\pm \rightarrow K^\pm\pi^+\pi^-J/\psi$ decays*, Phys. Rev. Lett. **91** (2003) 262001, [arXiv:hep-ex/0309032](#).
- [8] Belle collaboration, S. K. Choi *et al.*, *Observation of a resonance-like structure in the $\pi^\pm\psi'$ mass distribution in exclusive $B \rightarrow K\pi^\pm\psi'$ decays*, Phys. Rev. Lett. **100** (2008) 142001, [arXiv:0708.1790](#).
- [9] LHCb collaboration, R. Aaij *et al.*, *Observation of $J/\psi p$ resonances consistent with pentaquark states in $\Lambda_b^0 \rightarrow J/\psi p K^-$ decays*, Phys. Rev. Lett. **115** (2015) 072001, [arXiv:1507.03414](#).
- [10] LHCb collaboration, R. Aaij *et al.*, *Model-independent evidence for $J/\psi p$ contributions to $\Lambda_b^0 \rightarrow J/\psi p K^-$ decays*, Phys. Rev. Lett. **117** (2016) 082002, [arXiv:1604.05708](#).
- [11] LHCb collaboration, R. Aaij *et al.*, *Observation of a narrow pentaquark state, $P_c(4312)^+$, and of two-peak structure of the $P_c(4450)^+$* , Phys. Rev. Lett. **122** (2019) 222001, [arXiv:1904.03947](#).
- [12] LHCb collaboration, R. Aaij *et al.*, *Observation of an exotic narrow doubly charmed tetraquark*, Nature Physics **18** (2022) 751, [arXiv:2109.01038](#).
- [13] LHCb collaboration, R. Aaij *et al.*, *Study of the doubly charmed tetraquark T_{cc}^+* , Nature Communications **13** (2022) 3351, [arXiv:2109.01056](#).
- [14] F. E. Close and P. R. Page, *The $D^{*0}\bar{D}^0$ threshold resonance*, Phys. Lett. **B578** (2004) 119, [arXiv:hep-ph/0309253](#).
- [15] M. Karliner and J. L. Rosner, *New exotic meson and baryon resonances from doubly-heavy hadronic molecules*, Phys. Rev. Lett. **115** (2015) 122001, [arXiv:1506.06386](#).

- [16] L. Maiani, F. Piccinini, A. D. Polosa, and V. Riquer, *Diquark-antidiquarks with hidden or open charm and the nature of $X(3872)$* , Phys. Rev. **D71** (2005) 014028, arXiv:hep-ph/0412098.
- [17] L. Maiani, A. D. Polosa, and V. Riquer, *The new pentaquarks in the diquark model*, Phys. Lett. **B749** (2015) 289, arXiv:1507.04980.
- [18] S. Dubynskiy and M. B. Voloshin, *Hadro-charmonium*, Phys. Lett. **B666** (2008) 344, arXiv:0803.2224.
- [19] D. V. Bugg, *An explanation of Belle states $Z_b(10610)$ and $Z_b(10650)$* , EPL **96** (2011) 11002, arXiv:1105.5492.
- [20] P. Pakhlov and T. Uglov, *Charged charmonium-like $Z^+(4430)$ from rescattering in conventional B decays*, Phys. Lett. **B748** (2015) 183, arXiv:1408.5295.
- [21] G. Yang, J. Ping, and J. Segovia, *Doubly charmed pentaquarks*, Phys. Rev. **D101** (2020) .
- [22] M. Padmanath, R. G. Edwards, N. Mathur, and M. Peardon, *Spectroscopy of doubly and triply-charmed baryons from lattice QCD*, PoS **LATTICE2013** (2014) 247, arXiv:1311.4354.
- [23] LHCb collaboration, A. A. Alves Jr. *et al.*, *The LHCb detector at the LHC*, JINST **3** (2008) S08005.
- [24] LHCb collaboration, R. Aaij *et al.*, *LHCb detector performance*, Int. J. Mod. Phys. **A30** (2015) 1530022, arXiv:1412.6352.
- [25] R. Aaij *et al.*, *Performance of the LHCb trigger and full real-time reconstruction in Run 2 of the LHC*, JINST **14** (2019) P04013, arXiv:1812.10790.
- [26] S. Borghi, *Novel real-time alignment and calibration of the LHCb detector and its performance*, Nucl. Instrum. Meth. **A845** (2017) 560.
- [27] R. Aaij *et al.*, *The LHCb trigger and its performance in 2011*, JINST **8** (2013) P04022, arXiv:1211.3055.
- [28] R. Aaij *et al.*, *Tesla: an application for real-time data analysis in high energy physics*, Comput. Phys. Commun. **208** (2016) 35, arXiv:1604.05596.
- [29] T. Sjöstrand, S. Mrenna, and P. Skands, *PYTHIA 6.4 physics and manual*, JHEP **05** (2006) 026, arXiv:hep-ph/0603175; T. Sjöstrand, S. Mrenna, and P. Skands, *A brief introduction to PYTHIA 8.1*, Comput. Phys. Commun. **178** (2008) 852, arXiv:0710.3820.
- [30] I. Belyaev *et al.*, *Handling of the generation of primary events in Gauss, the LHCb simulation framework*, J. Phys. Conf. Ser. **331** (2011) 032047.
- [31] D. J. Lange, *The EvtGen particle decay simulation package*, Nucl. Instrum. Meth. **A462** (2001) 152.

- [32] P. Golonka and Z. Was, *PHOTOS Monte Carlo: A precision tool for QED corrections in Z and W decays*, Eur. Phys. J. **C45** (2006) 97, [arXiv:hep-ph/0506026](#).
- [33] Geant4 collaboration, J. Allison *et al.*, *Geant4 developments and applications*, IEEE Trans. Nucl. Sci. **53** (2006) 270; Geant4 collaboration, S. Agostinelli *et al.*, *Geant4: A simulation toolkit*, Nucl. Instrum. Meth. **A506** (2003) 250.
- [34] M. Clemencic *et al.*, *The LHCb simulation application, Gauss: Design, evolution and experience*, J. Phys. Conf. Ser. **331** (2011) 032023.
- [35] LHCb collaboration, R. Aaij *et al.*, *Observation of new Ξ_c^0 baryons decaying to $\Lambda_c^+ K^-$* , Phys. Rev. Lett. **124** (2020) 222001, [arXiv:2003.13649](#).
- [36] A. Hoecker *et al.*, *TMVA 4 — Toolkit for Multivariate Data Analysis with ROOT. Users Guide.*, [arXiv:physics/0703039](#).
- [37] T. Skwarnicki, *A study of the radiative cascade transitions between the Upsilon-prime and Upsilon resonances*, PhD thesis, Institute of Nuclear Physics, Krakow, 1986, DESY-F31-86-02.
- [38] E. Gross and O. Vitells, *Trial factors for the look elsewhere effect in high energy physics*, Eur. Phys. J. **C70** (2010) 525, [arXiv:1005.1891](#).
- [39] Particle Data Group, R. L. Workman *et al.*, *Review of particle physics*, Prog. Theor. Exp. Phys. **2022** (2022) 083C01.

LHCb collaboration

R. Aaij³³ , A.S.W. Abdelmotteleb⁵² , C. Abellan Beteta⁴⁶ , F. Abudinén⁵² ,
 T. Ackernley⁵⁶ , B. Adeva⁴² , M. Adinolfi⁵⁰ , P. Adlarson⁷⁸ , H. Afsharnia¹⁰ ,
 C. Agapopoulou⁴⁴ , C.A. Aidala⁷⁹ , Z. Ajaltouni¹⁰ , S. Akar⁶¹ , K. Akiba³³ ,
 P. Albicocco²⁴ , J. Albrecht¹⁶ , F. Alessio⁴⁴ , M. Alexander⁵⁵ , A. Alfonso Albero⁴¹ ,
 Z. Aliouche⁵⁸ , P. Alvarez Cartelle⁵¹ , R. Amalric¹⁴ , S. Amato² , J.L. Amey⁵⁰ ,
 Y. Amhis^{12,44} , L. An⁵ , L. Anderlini²³ , M. Andersson⁴⁶ , A. Andreianov³⁹ , P. A.
 Andreola⁴⁶ , M. Andreotti²² , D. Andreou⁶⁴ , D. Ao⁶ , F. Archilli^{32,u} ,
 S.A Arguedas Cuendis⁸ , A. Artamonov³⁹ , M. Artuso⁶⁴ , E. Aslanides¹¹ ,
 M. Atzeni⁶⁰ , B. Audurier¹³ , D. Bacher⁵⁹ , I.B Bachiller Perea⁹ , S. Bachmann¹⁸ ,
 M. Bachmayer⁴⁵ , J.J. Back⁵² , A. Bailly-reyre¹⁴ , P. Baladron Rodriguez⁴² ,
 V. Balagura¹³ , W. Baldini^{22,44} , J. Baptista de Souza Leite¹ , M. Barbetti^{23,k} , I.
 R. Barbosa⁶⁶ , R.J. Barlow⁵⁸ , S. Barsuk¹² , W. Barter⁵⁴ , M. Bartolini⁵¹ ,
 F. Baryshnikov³⁹ , J.M. Basels¹⁵ , G. Bassi^{30,r} , B. Batsukh⁴ , A. Battig¹⁶ ,
 A. Bay⁴⁵ , A. Beck⁵² , M. Becker¹⁶ , F. Bedeschi³⁰ , I.B. Bediaga¹ , A. Beiter⁶⁴ ,
 S. Belin⁴² , V. Bellec⁴⁶ , K. Belous³⁹ , I. Belov²⁵ , I. Belyaev³⁹ , G. Benane¹¹ ,
 G. Bencivenni²⁴ , E. Ben-Haim¹⁴ , A. Berezhnoy³⁹ , R. Bernet⁴⁶ , S. Bernet Andres⁴⁰ ,
 D. Berninghoff¹⁸ , H.C. Bernstein⁶⁴ , C. Bertella⁵⁸ , A. Bertolin²⁹ , C. Betancourt⁴⁶ ,
 F. Betti⁵⁴ , J. B. Bex⁵¹ , I.a. Bezshyiko⁴⁶ , J. Bhom³⁶ , L. Bian⁷⁰ , M.S. Bieker¹⁶ ,
 N.V. Biesuz²² , P. Billoir¹⁴ , A. Biolchini³³ , M. Birch⁵⁷ , F.C.R. Bishop⁵¹ ,
 A. Bitadze⁵⁸ , A. Bizzeti , M.P. Blago⁵¹ , T. Blake⁵² , F. Blanc⁴⁵ , J.E. Blank¹⁶ ,
 S. Blusk⁶⁴ , D. Bobulska⁵⁵ , V.B Bocharnikov³⁹ , J.A. Boelhauve¹⁶ ,
 O. Boente Garcia¹³ , T. Boettcher⁶¹ , A. Bohare⁵⁴ , A. Boldyrev³⁹ , C.S. Bolognani⁷⁶ ,
 R. Bolzonella^{22,j} , N. Bondar³⁹ , F. Borgato^{29,44} , S. Borghi⁵⁸ , M. Borsato¹⁸ ,
 J.T. Borsuk³⁶ , S.A. Bouchiba⁴⁵ , T.J.V. Bowcock⁵⁶ , A. Boyer⁴⁴ , C. Bozzi²² ,
 M.J. Bradley⁵⁷ , S. Braun⁶² , A. Brea Rodriguez⁴² , N. Breer¹⁶ , J. Brodzicka³⁶ ,
 A. Brossa Gonzalo⁴² , J. Brown⁵⁶ , D. Brundu²⁸ , A. Buonauro⁴⁶ , L. Buonincontri²⁹ ,
 A.T. Burke⁵⁸ , C. Burr⁴⁴ , A. Bursche⁶⁸ , A. Butkevich³⁹ , J.S. Butter³³ ,
 J. Buytaert⁴⁴ , W. Byczynski⁴⁴ , S. Cadeddu²⁸ , H. Cai⁷⁰ , R. Calabrese^{22,j} ,
 L. Calefice¹⁶ , S. Cali²⁴ , M. Calvi^{27,n} , M. Calvo Gomez⁴⁰ , J.C Cambon Bouzas⁴² ,
 P. Campana²⁴ , D.H. Campora Perez⁷⁶ , A.F. Campoverde Quezada⁶ , S. Capelli^{27,n} ,
 L. Capriotti²² , A. Carbone^{21,h} , L.C Carcedo Salgado⁴² , R. Cardinale^{25,l} ,
 A. Cardini²⁸ , P. Carniti^{27,n} , L. Carus¹⁸ , A. Casais Vidal⁴² , R. Caspary¹⁸ ,
 G. Casse⁵⁶ , M. Cattaneo⁴⁴ , G. Cavallero²² , V. Cavallini^{22,j} , S. Celani⁴⁵ ,
 J. Cerasoli¹¹ , D. Cervenkov⁵⁹ , S. Cesare^{26,m} , A.J. Chadwick⁵⁶ , I. Chahrour⁷⁹ ,
 M.G. Chapman⁵⁰ , M. Charles¹⁴ , Ph. Charpentier⁴⁴ , C.A. Chavez Barajas⁵⁶ ,
 M. Chefdeville⁹ , C. Chen¹¹ , S. Chen⁴ , A. Chernov³⁶ , S. Chernyshenko⁴⁸ ,
 V. Chobanova^{42,x} , S. Cholak⁴⁵ , M. Chruszcz³⁶ , A. Chubykin³⁹ , V. Chulikov³⁹ ,
 P. Ciambone²⁴ , M.F. Cicala⁵² , X. Cid Vidal⁴² , G. Ciezarek⁴⁴ , P. Cifra⁴⁴ ,
 G. Ciullo^{j,22} , P.E.L. Clarke⁵⁴ , M. Clemencic⁴⁴ , H.V. Cliff⁵¹ , J. Closier⁴⁴ ,
 J.L. Cobbledick⁵⁸ , C. Cocha Toapaxi¹⁸ , V. Coco⁴⁴ , J. Cogan¹¹ , E. Cogneras¹⁰ ,
 L. Cojocariu³⁸ , P. Collins⁴⁴ , T. Colombo⁴⁴ , A. Comerma-Montells⁴¹ , L. Congedo²⁰ ,
 A. Contu²⁸ , N. Cooke⁵⁵ , I. Corredoira⁴² , G. Corti⁴⁴ , J.J. Cottee Meldrum⁵⁰ ,
 B. Couturier⁴⁴ , D.C. Craik⁴⁶ , M. Cruz Torres^{1,f} , R. Currie⁵⁴ , C.L. Da Silva⁶³ ,
 S. Dadabaev³⁹ , L. Dai⁶⁷ , X. Dai⁵ , E. Dall’Occo¹⁶ , J. Dalseno⁴² ,
 C. D’Ambrosio⁴⁴ , J. Daniel¹⁰ , A. Danilina³⁹ , P. d’Argent²⁰ , A. Davidson⁵² ,
 J.E. Davies⁵⁸ , A. Davis⁵⁸ , O. De Aguiar Francisco⁵⁸ , C. De Angelis²⁸ , J. de Boer³³ ,
 K. De Bruyn⁷⁵ , S. De Capua⁵⁸ , M. De Cian¹⁸ , U. De Freitas Carneiro Da Graca^{1,b} ,
 E. De Lucia²⁴ , J.M. De Miranda¹ , L. De Paula² , M. De Serio^{20,g} , D. De Simone⁴⁶ ,

C. Vázquez Sierra⁴² , S. Vecchi²² , J.J. Velthuis⁵⁰ , M. Veltri^{23,v} , A. Venkateswaran⁴⁵ ,
M. Vesterinen⁵² , D. Vieira⁶¹ , M. Vieites Diaz⁴⁴ , X. Vilasis-Cardona⁴⁰ ,
E. Vilella Figueras⁵⁶ , A. Villa²¹ , P. Vincent¹⁴ , F.C. Volle¹² , D. vom Bruch¹¹ ,
V. Vorobyev³⁹ , N. Voropaev³⁹ , K. Vos⁷⁶ , C. Vrahas⁵⁴ , J. Walsh³⁰ , E.J. Walton⁶⁵ ,
G. Wan⁵ , C. Wang¹⁸ , G. Wang⁷ , J. Wang⁵ , J. Wang⁴ , J. Wang³ , J. Wang⁷⁰ ,
M. Wang²⁶ , N. W. Wang⁶ , R. Wang⁵⁰ , X. Wang⁶⁸ , Y. Wang⁷ , Z. Wang⁴⁶ ,
Z. Wang³ , Z. Wang⁶ , J.A. Ward^{52,65} , N.K. Watson⁴⁹ , D. Websdale⁵⁷ , Y. Wei⁵ ,
B.D.C. Westhenry⁵⁰ , D.J. White⁵⁸ , M. Whitehead⁵⁵ , A.R. Wiederhold⁵² ,
D. Wiedner¹⁶ , G. Wilkinson⁵⁹ , M.K. Wilkinson⁶¹ , I. Williams⁵¹ , M. Williams⁶⁰ ,
M.R.J. Williams⁵⁴ , R. Williams⁵¹ , F.F. Wilson⁵³ , W. Wislicki³⁷ , M. Witek³⁶ ,
L. Witola¹⁸ , C.P. Wong⁶³ , G. Wormser¹² , S.A. Wotton⁵¹ , H. Wu⁶⁴ , J. Wu⁷ ,
Y. Wu⁵ , K. Wyllie⁴⁴ , S. Xian⁶⁸ , Z. Xiang⁶ , Y. Xie⁷ , A. Xu³⁰ , J. Xu⁶ , L. Xu³ ,
L. Xu³ , M. Xu⁵² , Z. Xu¹⁰ , Z. Xu⁶ , Z. Xu⁴ , D. Yang³ , S. Yang⁶ , X. Yang⁵ ,
Y. Yang²⁵ , Z. Yang⁵ , Z. Yang⁶² , V. Yeroshenko¹² , H. Yeung⁵⁸ , H. Yin⁷ , C. Y.
Yu⁵ , J. Yu⁶⁷ , X. Yuan⁴ , Z. Y. Yuan⁵ , E. Zaffaroni⁴⁵ , M. Zavertyaev¹⁷ ,
M. Zdybal³⁶ , M. Zeng³ , C. Zhang⁵ , D. Zhang⁷ , J. Zhang⁶ , L. Zhang³ ,
S. Zhang⁶⁷ , S. Zhang⁵ , Y. Zhang⁵ , Y. Zhang⁵⁹ , Y. Z. Zhang³ , Y. Zhao¹⁸ ,
A. Zharkova³⁹ , A. Zhelezov¹⁸ , X. Z. Zheng³ , Y. Zheng⁶ , T. Zhou⁵ , X. Zhou⁷ ,
Y. Zhou⁶ , V. Zhovkovska¹² , L. Z. Zhu⁶ , X. Zhu³ , X. Zhu⁷ , Z. Zhu⁶ ,
V. Zhukov^{15,39} , J. Zhuo⁴³ , Q. Zou^{4,6} , S. Zucchelli^{21,h} , D. Zuliani²⁹ , G. Zunica⁵⁸ .

¹Centro Brasileiro de Pesquisas Físicas (CBPF), Rio de Janeiro, Brazil

²Universidade Federal do Rio de Janeiro (UFRJ), Rio de Janeiro, Brazil

³Center for High Energy Physics, Tsinghua University, Beijing, China

⁴Institute Of High Energy Physics (IHEP), Beijing, China

⁵School of Physics State Key Laboratory of Nuclear Physics and Technology, Peking University, Beijing, China

⁶University of Chinese Academy of Sciences, Beijing, China

⁷Institute of Particle Physics, Central China Normal University, Wuhan, Hubei, China

⁸Consejo Nacional de Rectores (CONARE), San Jose, Costa Rica

⁹Université Savoie Mont Blanc, CNRS, IN2P3-LAPP, Annecy, France

¹⁰Université Clermont Auvergne, CNRS/IN2P3, LPC, Clermont-Ferrand, France

¹¹Aix Marseille Univ, CNRS/IN2P3, CPPM, Marseille, France

¹²Université Paris-Saclay, CNRS/IN2P3, IJCLab, Orsay, France

¹³Laboratoire Leprince-Ringuet, CNRS/IN2P3, Ecole Polytechnique, Institut Polytechnique de Paris, Palaiseau, France

¹⁴LPNHE, Sorbonne Université, Paris Diderot Sorbonne Paris Cité, CNRS/IN2P3, Paris, France

¹⁵I. Physikalisches Institut, RWTH Aachen University, Aachen, Germany

¹⁶Fakultät Physik, Technische Universität Dortmund, Dortmund, Germany

¹⁷Max-Planck-Institut für Kernphysik (MPIK), Heidelberg, Germany

¹⁸Physikalisches Institut, Ruprecht-Karls-Universität Heidelberg, Heidelberg, Germany

¹⁹School of Physics, University College Dublin, Dublin, Ireland

²⁰INFN Sezione di Bari, Bari, Italy

²¹INFN Sezione di Bologna, Bologna, Italy

²²INFN Sezione di Ferrara, Ferrara, Italy

²³INFN Sezione di Firenze, Firenze, Italy

²⁴INFN Laboratori Nazionali di Frascati, Frascati, Italy

²⁵INFN Sezione di Genova, Genova, Italy

²⁶INFN Sezione di Milano, Milano, Italy

²⁷INFN Sezione di Milano-Bicocca, Milano, Italy

²⁸INFN Sezione di Cagliari, Monserrato, Italy

²⁹Università degli Studi di Padova, Università e INFN, Padova, Padova, Italy

³⁰INFN Sezione di Pisa, Pisa, Italy

³¹INFN Sezione di Roma La Sapienza, Roma, Italy

- ³² INFN Sezione di Roma Tor Vergata, Roma, Italy
- ³³ Nikhef National Institute for Subatomic Physics, Amsterdam, Netherlands
- ³⁴ Nikhef National Institute for Subatomic Physics and VU University Amsterdam, Amsterdam, Netherlands
- ³⁵ AGH - University of Science and Technology, Faculty of Physics and Applied Computer Science, Kraków, Poland
- ³⁶ Henryk Niewodniczanski Institute of Nuclear Physics Polish Academy of Sciences, Kraków, Poland
- ³⁷ National Center for Nuclear Research (NCBJ), Warsaw, Poland
- ³⁸ Horia Hulubei National Institute of Physics and Nuclear Engineering, Bucharest-Magurele, Romania
- ³⁹ Affiliated with an institute covered by a cooperation agreement with CERN
- ⁴⁰ DS4DS, La Salle, Universitat Ramon Llull, Barcelona, Spain
- ⁴¹ ICCUB, Universitat de Barcelona, Barcelona, Spain
- ⁴² Instituto Galego de Física de Altas Enerxías (IGFAE), Universidade de Santiago de Compostela, Santiago de Compostela, Spain
- ⁴³ Instituto de Física Corpuscular, Centro Mixto Universidad de Valencia - CSIC, Valencia, Spain
- ⁴⁴ European Organization for Nuclear Research (CERN), Geneva, Switzerland
- ⁴⁵ Institute of Physics, Ecole Polytechnique Fédérale de Lausanne (EPFL), Lausanne, Switzerland
- ⁴⁶ Physik-Institut, Universität Zürich, Zürich, Switzerland
- ⁴⁷ NSC Kharkiv Institute of Physics and Technology (NSC KIPT), Kharkiv, Ukraine
- ⁴⁸ Institute for Nuclear Research of the National Academy of Sciences (KINR), Kyiv, Ukraine
- ⁴⁹ University of Birmingham, Birmingham, United Kingdom
- ⁵⁰ H.H. Wills Physics Laboratory, University of Bristol, Bristol, United Kingdom
- ⁵¹ Cavendish Laboratory, University of Cambridge, Cambridge, United Kingdom
- ⁵² Department of Physics, University of Warwick, Coventry, United Kingdom
- ⁵³ STFC Rutherford Appleton Laboratory, Didcot, United Kingdom
- ⁵⁴ School of Physics and Astronomy, University of Edinburgh, Edinburgh, United Kingdom
- ⁵⁵ School of Physics and Astronomy, University of Glasgow, Glasgow, United Kingdom
- ⁵⁶ Oliver Lodge Laboratory, University of Liverpool, Liverpool, United Kingdom
- ⁵⁷ Imperial College London, London, United Kingdom
- ⁵⁸ Department of Physics and Astronomy, University of Manchester, Manchester, United Kingdom
- ⁵⁹ Department of Physics, University of Oxford, Oxford, United Kingdom
- ⁶⁰ Massachusetts Institute of Technology, Cambridge, MA, United States
- ⁶¹ University of Cincinnati, Cincinnati, OH, United States
- ⁶² University of Maryland, College Park, MD, United States
- ⁶³ Los Alamos National Laboratory (LANL), Los Alamos, NM, United States
- ⁶⁴ Syracuse University, Syracuse, NY, United States
- ⁶⁵ School of Physics and Astronomy, Monash University, Melbourne, Australia, associated to ⁵²
- ⁶⁶ Pontifícia Universidade Católica do Rio de Janeiro (PUC-Rio), Rio de Janeiro, Brazil, associated to ²
- ⁶⁷ Physics and Micro Electronic College, Hunan University, Changsha City, China, associated to ⁷
- ⁶⁸ Guangdong Provincial Key Laboratory of Nuclear Science, Guangdong-Hong Kong Joint Laboratory of Quantum Matter, Institute of Quantum Matter, South China Normal University, Guangzhou, China, associated to ³
- ⁶⁹ Lanzhou University, Lanzhou, China, associated to ⁴
- ⁷⁰ School of Physics and Technology, Wuhan University, Wuhan, China, associated to ³
- ⁷¹ Departamento de Física, Universidad Nacional de Colombia, Bogota, Colombia, associated to ¹⁴
- ⁷² Universität Bonn - Helmholtz-Institut für Strahlen und Kernphysik, Bonn, Germany, associated to ¹⁸
- ⁷³ Eotvos Lorand University, Budapest, Hungary, associated to ⁴⁴
- ⁷⁴ INFN Sezione di Perugia, Perugia, Italy, associated to ²²
- ⁷⁵ Van Swinderen Institute, University of Groningen, Groningen, Netherlands, associated to ³³
- ⁷⁶ Universiteit Maastricht, Maastricht, Netherlands, associated to ³³
- ⁷⁷ Tadeusz Kosciuszko Cracow University of Technology, Cracow, Poland, associated to ³⁶
- ⁷⁸ Department of Physics and Astronomy, Uppsala University, Uppsala, Sweden, associated to ⁵⁵
- ⁷⁹ University of Michigan, Ann Arbor, MI, United States, associated to ⁶⁴
- ⁸⁰ Departement de Physique Nucleaire (SPhN), Gif-Sur-Yvette, France

^a Universidade de Brasília, Brasília, Brazil

^b Centro Federal de Educação Tecnológica Celso Suckow da Fonseca, Rio De Janeiro, Brazil

- ^c *Central South U., Changsha, China*
- ^d *Hangzhou Institute for Advanced Study, UCAS, Hangzhou, China*
- ^e *Excellence Cluster ORIGINS, Munich, Germany*
- ^f *Universidad Nacional Autónoma de Honduras, Tegucigalpa, Honduras*
- ^g *Università di Bari, Bari, Italy*
- ^h *Università di Bologna, Bologna, Italy*
- ⁱ *Università di Cagliari, Cagliari, Italy*
- ^j *Università di Ferrara, Ferrara, Italy*
- ^k *Università di Firenze, Firenze, Italy*
- ^l *Università di Genova, Genova, Italy*
- ^m *Università degli Studi di Milano, Milano, Italy*
- ⁿ *Università di Milano Bicocca, Milano, Italy*
- ^o *Università di Modena e Reggio Emilia, Modena, Italy*
- ^p *Università di Padova, Padova, Italy*
- ^q *Università di Perugia, Perugia, Italy*
- ^r *Scuola Normale Superiore, Pisa, Italy*
- ^s *Università di Pisa, Pisa, Italy*
- ^t *Università della Basilicata, Potenza, Italy*
- ^u *Università di Roma Tor Vergata, Roma, Italy*
- ^v *Università di Urbino, Urbino, Italy*
- ^w *Universidad de Alcalá, Alcalá de Henares , Spain*
- ^x *Universidade da Coruña, Coruña, Spain*